Periodic variation in the I- and Ag-projectile $L\beta_1$-to-$L\alpha$ x-ray intensity ratio with the target atomic number

Amal K. Saha,[1] B. B. Dhal,[2] U. Tiwari,[1] M. B. Kurup,[1] H. C. Padhi,[2] K. G. Prasad,[1] and P. N. Tandon[1]
[1]*Tata Institute of Fundamental Research, Homi Bhabha Road, Mumbai 400 005, India*
[2]*Institute of Physics, Sachivalaya Marg, Bhubaneswar 751005, India*
(Received 5 September 1997; revised manuscript received 29 January 1998)

Periodic variation in the $L\beta_1$-to-$L\alpha$ x-ray intensity ratio of I and Ag projectiles has been observed as a function of the atomic number Z_2 of the collision partner. It is shown that this periodic behavior is linked to the enhanced intensity of the $L\beta_3$ and $L\beta_4$ x-ray components, which are not resolved from the dominant $L\beta_1$ x ray. The enhancement of the $L\beta_3$ and $L\beta_4$ components is attributed to the increased L_1-subshell ionization via molecular orbitals. The x-ray intensity ratio is also found to be nearly the same, in a few selected cases studied, irrespective of the role of the emitter as target or projectile. [S1050-2947(98)05606-6]

PACS number(s): 34.50.Fa, 34.50.Gb

I. INTRODUCTION

Extensive studies have been carried out in the past to understand the ionization of inner shells of target atoms in collisions with energetic light ions [1–3]. The experimental data obtained, particularly for the ionization of the K shell of the target atoms using proton beams, have been of immense help in the improvement of the theoretical models. An extensive study of the existing K-shell data was performed by Paul and Muhr [4] and also by Lapicki [5]. The ECPSSR calculations [3], which include energy loss of the projectile (E), its Coulombic deflection (C), target polarization within the perturbed stationary state (PSS) approximation and the relativistic (R) correction, explain the K-shell ionization cross-section data involving light ions extremely well [4,5]. The situation though is not so good when heavier projectiles are used and large discrepancies in the observed cross sections have been observed [6,7].

In contrast to the K-shell ionization data, significant deviations in the L-shell ionization cross sections have been observed from the ECPSSR theory [2,8–11]. A part of the discrepancy may be associated with the difficulties in the deduction of the L-subshell ionization cross section from the complex L x-ray spectra since all its components are not well resolved due to comparatively poor resolution of the Si (Li) detectors used in most experiments. The reliability of the L-subshell data is further limited because of the uncertainties in the use of the atomic parameters, which are affected by multiple vacancy production in outer shells. These atomic parameters are needed to convert the yield of different x-ray lines into subshell ionization cross section. In addition, theoretical complications also do arise in the case of L-subshell ionization (which are absent in the case of K shell), particularly when using heavier ion beams. This is because the ionization of one subshell cannot be regarded as independent from the ionization of the other subshells in view of the small energy separation between the L subshells and the large Coulomb field of the incident projectile. Consequently, additional effects, such as the intrashell transitions induced between the subshells by the projectile in the same atomic collision have to be considered [8,10,12–16].

Compared to the target L-subshell ionization, detailed studies on the projectile L-subshell ionization are very much limited. In one of the earlier studies conducted by Datz *et al.* [17], large periodic variation in the relative number of the L-subshell vacancies of the iodine projectile, in the energy range 15–60 MeV, was observed as a function of the atomic number Z_2 of the collision partner. These authors observed strong variation in the projectile L x-ray intensity ratio $L\beta_1$ to $L\alpha$ as a function of Z_2 between 6 and 82. Hagmann *et al.* [18] have also observed similar results for iodine projectile impinging on selected targets between Ag and U. Qualitative understanding of these periodic variations were made in terms of the radial coupling of the adiabatic molecular orbitals (MO), linked to the crossing of various L subshells of the iodine projectile with the K, L, or M shell of the target atom, during the collision. The strong variation of the $L\beta_1$-to-$L\alpha$ intensity ratio reported by Datz *et al.* [17] for $6 \leqslant Z_2 \leqslant 16$ is somewhat intriguing as one does not expect overlap of the iodine L levels with any levels in this low-Z_2 region. In order to get more information on the strong target as well as energy-dependent $L\beta_1$-to-$L\alpha$ intensity ratios of the projectile, we have carried out similar measurements using an iodine projectile in a still higher range of energies. Furthermore, thin targets have been used in contrast with the thick targets used in the earlier measurements [17]. We have further carried out measurements on Ag x rays with Ag as a projectile and also as a target, with Se and Ni collision partners so that the same united atom is formed in the two cases. We present here the results observed that not only support the earlier results observed by Datz *et al.* [17] but further reveal new features at higher impact energies used.

II. EXPERIMENTAL DETAILS

The layout of the experimental setup has been described elsewhere [7]. In brief, ion beams of ^{127}I, ^{107}Ag, ^{80}Se, and ^{56}Ni were obtained from the BARC-TIFR Pelletron accelerator at Mumbai. A postaccelerator foil stripper [19] had to be used to further strip the ^{127}I and ^{107}Ag ions to allow them to bend into the 30° beam line. The charge selected beam (between 19^+ and 22^+, depending on the energy of the

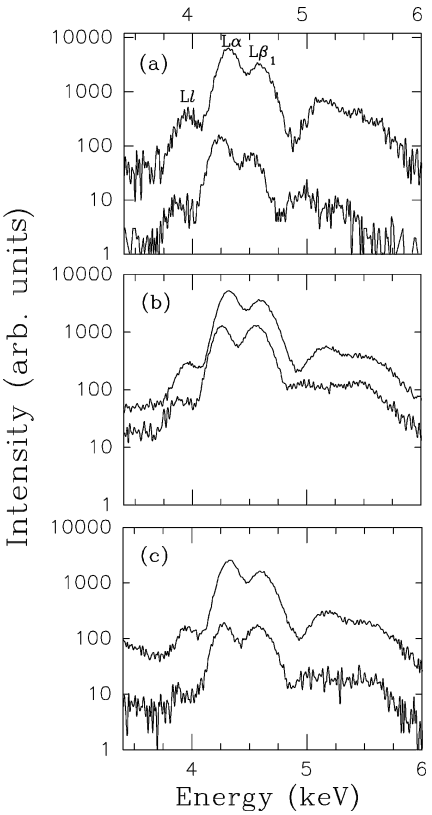

FIG. 1. Typical L x rays from the I projectile incident on thin targets of (a) C, (b) Ni, and (c) Yb. The upper lines are for impact energy 156 MeV and the lower lines for 63 MeV.

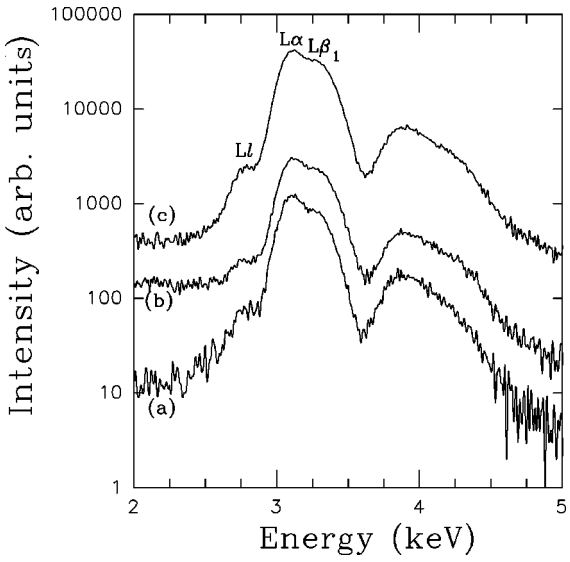

FIG. 2. Typical L x rays from 110 MeV Ag projectile incident on thin targets of (a) C, (b) Yb, and (c) Ni.

beam, for both the ions) was collimated using two adjustable beam-defining slits kept 1 m apart and nearly 1 m before the scattering chamber. The collimated beam of a few hundred pA intensity was made to impinge on various targets, mounted on a target wheel, whose position can be remotely controlled [20]. The targets used were ~ 25 μg/cm^2 thick and were made by evaporation of the target material on self-supporting C foils of thickness varying between 10 and 15 μg/cm^2. A Si (Li) x-ray detector (30-mm^2 sensitive area), energy resolution 170 eV at 5.9 keV, was placed at a distance of 10 cm outside the scattering chamber and at an angle of 90° with respect to the beam direction. The detector was isolated from the chamber vacuum by using a 25-μm mylar foil. The count rate in the detector was kept below 500 counts/s. The gain of the detector system was adjusted to ~ 10 eV/channel. The detector was calibrated using standard radioactive sources. Gain shifts were found to be $\leqslant 10$ eV in the course of the experiments. For additional measurements involving ^{80}Se, ^{56}Ni, and ^{107}Ag projectiles, no further charge stripping was done and the ions were in comparatively lower charge state varying between 4^+ and 8^+.

III. RESULTS AND DISCUSSION

Typical x-ray spectra observed using I and Ag ions in the region of their L x rays are shown in Figs. 1 and 2, respectively. In the case of the I projectile, the Ll, $L\alpha$, and $L\beta_1$ x-ray peaks are quite well resolved while in the case of Ag ions they are not completely resolved. The changes in the shape of the L x-ray spectra, as a function of the target and energy, are clearly depicted in the observed spectra (see Figs. 1 and 2). In order to obtain the intensities of the respective L x-ray transitions, the spectra were fitted using a multi-Gaussian fitting program, which can fit simultaneously up to twelve x-ray lines. The widths of each of the lines and their intensities could be independently varied. The whole region of the x-ray spectra was used for fitting purposes. This ensured minimum uncertainties in the underlying background in the x-ray peaks of interest arising because of the several overlapping transitions. A linear background was assumed while fitting the spectra. The reduced χ^2 was around 1. The estimated maximum Doppler broadening due to the finite size of the detector placed at 90° with respect to the beam direction was much smaller (<5 eV) when compared to the measured widths of the x-ray peaks (180–200 eV). The intensity of the three transitions Ll, $L\alpha$, and $L\beta_1$, which were found to be free from large uncertainties as ascertained from the variation in the fitting parameters, was used for further analysis. Small corrections for relative variation of the photopeak efficiency of the detector as well as absorption in the mylar window were also applied. It may be mentioned that the $L\alpha$ peak is a composite of $L\alpha_1$ and $L\alpha_2$ and it was treated as one peak. Similarly, the $L\beta_1$ peak has within it contributions from $L\beta_3$ and $L\beta_4$. As had been done by Datz *et al.* [17] we have also treated these lines as one composite peak in fitting the spectra. No attempts were made to evaluate the intensity of the other $L\beta$ and $L\gamma$ components because of the larger width associated with the multiple vacancy production in the outer shells. The intensity ratios Ll to $L\alpha$ and $L\beta_1$ to $L\alpha$ along with the fitted width of the $L\alpha$ and $L\beta_1$ lines, as a function of the atomic number Z_2 of the target, are shown in Figs. 3–5 at some typical energies used for I and Ag projectiles. The intensity ratios $L\beta_1$ to $L\alpha$, as a function of the energy of the projectile, for a given target, are also shown in Fig. 6. The variation of the fitted widths of the $L\alpha$ and $L\beta_1$ lines of the projectile with the incident energy is shown in Fig. 7 for a few targets. Table I also shows the energy of the two L x-ray transitions for different targets

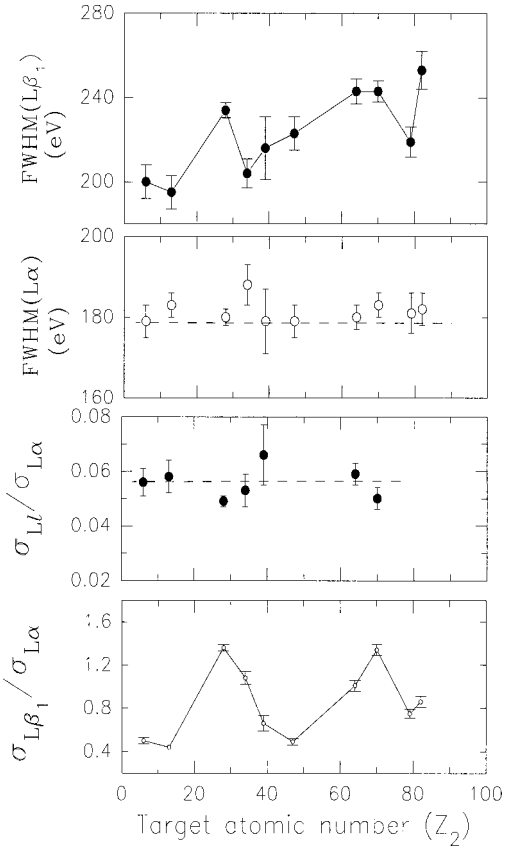

FIG. 3. The fitted $L\alpha$ and $L\beta_1$ x-ray linewidths (FWHM) and Ll-to-$L\alpha$ and $L\beta_1$-to-$L\alpha$ intensity ratios of 63-MeV I projectile incident on different targets. The lines drawn are to guide the eye only.

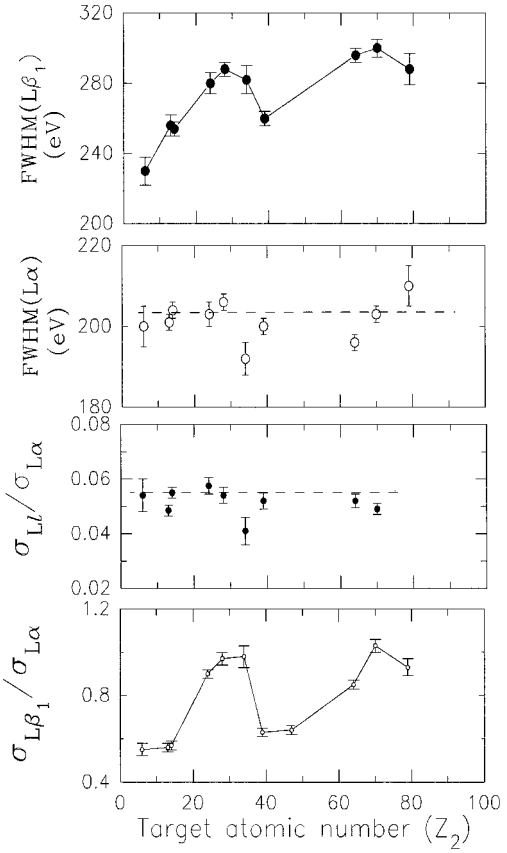

FIG. 4. Same as Fig. 3 for 120-MeV I projectile incident on different targets.

used in the experiment. Several important features have been observed, which are discussed below.

The average energy of the projectile $L\alpha$ and $L\beta_1$ x rays is found to be higher than that of the diagram lines by as much as 150 eV because of the multiple vacancies in the M shell of the projectile simultaneously present along with the L-shell vacancy. Additionally, the measured energies of the transitions, at a given projectile energy, are found to be insensitive to the atomic number of the collision partner. In fact, the variation in the energy of the $L\alpha$ peak at a given bombarding energy was within 5 to 10 eV for all the targets used. The only exception was the thin self-supporting C target, where the energy of the x ray was lower by $\sim$20 eV. This has been attributed to a lower average charge state of the I projectile in the self-supporting C target (thickness $\leqslant 15\ \mu g/cm^2$) as compared to the C backed targets (see below). The variation in the energy of the $L\beta_1$ x ray at a given bombarding energy was more than that of the $L\alpha$ x ray but remained within 10 to 20 eV for all the targets used. The insensitivity of the energy of the projectile L x rays to Z_2, at a given projectile energy, is consistent with the picture that the basic configuration of the ionized projectile at the time of x-ray emission is essentially the same for all the target projectile combinations as one expects the projectile charge state to have reached equilibrium in all the targets. Also at higher projectile energies used, the energy of the x rays is found to increase, which is also expected because of the higher ionization state of the projectile. The observed increase was up to 50 eV, for both $L\alpha$ and $L\beta_1$ transitions, for projectile energy varying between 63 and 180 MeV. The width of the $L\alpha$ peak was found to be fairly constant for different targets used (see Figs. 3–5). However, the widths of the $L\beta_1$ lines were about 25 to 30% larger than the $L\alpha$ line width and its variation as a function of the target was also quite significant, displaying nearly similar pattern as the intensity ratio $L\beta_1$ to $L\alpha$ (see Figs. 3–5), i.e., larger values at Ni, Gd, and Yb targets at which the intensity ratio $L\beta_1$ to $L\alpha$ is large.

The intensity ratios $L\beta_1$ to $L\alpha$ as a function of Z_2, shown in Figs. 3 and 4 for iodine at two incident energies and in Fig. 5 for silver projectile at 110 MeV, exhibit the oscillatory behavior reported earlier [17]. The nearly identical behavior in the position of the maxima and minima for the thick [17] and thin targets (present work) suggests their insensitivity to the charge state of the projectile, implying that equilibrium of the charge state has been reached. The ratio, Ll to $L\alpha$, on the other hand, remains constant at all the energies of the projectile used, at a constant value of about 5.5×10^{-2} in the case of iodine projectile. This ratio is found to have a value of $\sim 6.5\times10^{-2}$ for the Ag projectile. The oscillations in $L\beta_1$ to $L\alpha$ also persist with the Ag projectile exhibiting nearly identical pattern, not deviating much in the position of the maxima and the minima probably because Ag and I are very close as far as atomic number is concerned. However, in the case of 1.4 MeV/u Pb impinging on solid targets [21], Schönfeldt has observed a minimum at $Z_2\sim25$ and a maxi-

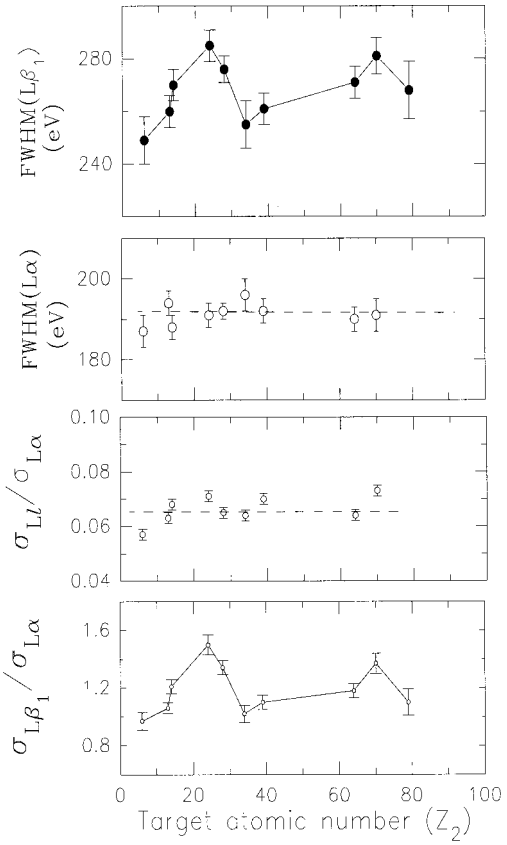

FIG. 5. Same as Fig. 3 for 110-MeV Ag projectile incident on different targets.

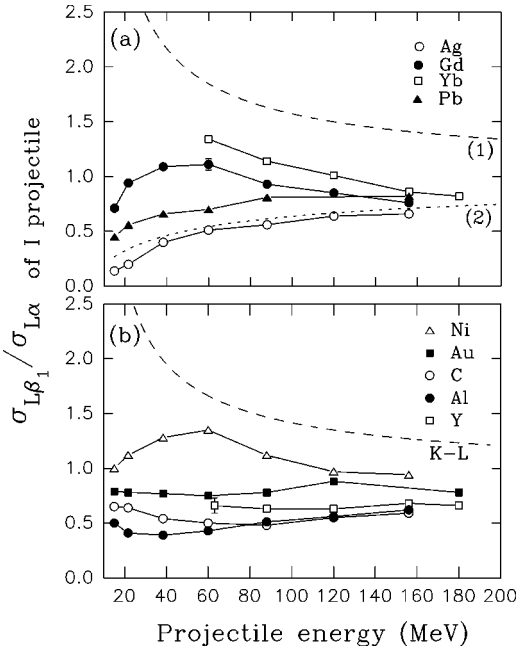

FIG. 6. The x-ray intensity ratio $L\beta_1$ to $L\alpha$ of the I projectile as a function of the impact energy for a number of targets. The data below 60 MeV are taken from Datz *et al.* [17] (shown after normalization at 60 MeV, see text). In (a), the dotted curve marked (1) is calculation based on [25] using MO correlation of Eichler *et al.* [28] for I→Gd,Yb (asymmetric collisions) and the dotted curve marked (2) is calculation based on [25] using MO correlation rule of Barat *et al.* [29] for I→Ag (near symmetric collision) . In (b), the dotted curve marked *K-L* is a model calculation based on Meyerhof *et al.* [26] using *K-L* level matching scheme for I→Ni. The errors in the data points are within the symbol size unless shown explicitly.

mum at $Z_2 \sim 50$ in the variation of the intensity ratio $L\beta_1$ to $L\alpha$ with Z_2, strongly suggesting projectile dependence. The Ll and $L\alpha$ x rays originate from the filling of a vacancy in the L_3 subshell and it is therefore not surprising that their ratio is independent of Z_2. Similar observation is made involving several other pairs of x-ray lines originating from the filling of the same L-subshell vacancy [17,21]. On the other hand, the unresolved $L\beta_1$, $L\beta_3$, and $L\beta_4$ x rays arise due to the filling of the vacancies in $L1$ and $L2$ subshells. The measured ratio $L\beta_1$ to $L\alpha$, therefore, involves all three subshells since $L\beta_3$ and $L\beta_4$ are not resolved from $L\beta_1$. The fitted widths of the $L\alpha$ and $L\beta_1$ lines as a function of Z_2 are also shown in Figs. 3–5. Since the $L\alpha$ linewidths are fairly constant and independent of Z_2 and the composite $L\beta_1$ linewidths show significant variation with Z_2, one may infer that the oscillatory behavior in the $L\beta_1$-to-$L\alpha$ ratio is linked to the width of the composite $L\beta_1$ line. Such a target-dependent variation in $L\beta_1$ linewidth might arise either due to the variation in the relative intensity of the unresolved components $L\beta_3$ and $L\beta_4$ or due to the spread in the energy of the $L\beta_1$ transition resulting from increased target-dependent multiple vacancies in the M shell. Since no significant variation is observed in the dependence of the $L\beta_1$ energy ($\leqslant 20$ eV) on Z_2, one may conclude that the variation in the width of the composite $L\beta_1$ line originates from the variation in the intensity of the unresolved $L\beta_3$ and $L\beta_4$ components. This explanation is strongly supported by the measured high-resolution x-ray spectra of 101.5-MeV iodine projectile incident on Cu (Budick *et al.* [22]), which lies on a maximum of the $L\beta_1$-to-$L\alpha$ intensity ratio (Fig. 3). These authors reported the intensities of the $L\beta_3$ and $L\beta_4$ transitions to be about 65% of that of $L\beta_1$ in contrast with the calculated value of ~40% [23]. The intensity of the $L\gamma_{2,3}$ transitions, originating from the L_1 subshell, is also found to be enhanced. The observed intensity ratio Ll to $L\alpha$ remains constant as Z_2 is varied, so an explanation for the observed periodic variation of the intensity ratio $L\beta_1$ to $L\alpha$ with Z_2 in terms of the selective M-subshell ionization is ruled out. It is therefore evident that the periodic variation in the intensity ratio $L\beta_1$ to $L\alpha$ is linked to the variation in the intensity of the $L\beta_3$ and $L\beta_4$ components, which would in turn imply either the dynamic rearrangement of the vacancy among the L subshells of the projectile (intrashell couplings) due to Coulomb perturbation of the collision partner [15] or Z_2-dependent periodic variation in the ionization of the L_1 subshell. Intrashell coupling calculations similar to [15] carried out for the present system do not predict the observed periodic variations [24].

The variation of the intensity ratio $L\beta_1$ to $L\alpha$ as a function of the projectile energy is shown in Fig. 6. The data of Datz *et al.* [17], which are in the projectile energy range 15–60 MeV and which were obtained using thick solid targets are also shown in Fig. 6 after normalizing to our data at 60 MeV. The agreement between our data and that of Datz *et al.* [17] at 63 and 60 MeV, respectively, is within 30%, which is reasonably good considering that the data obtained

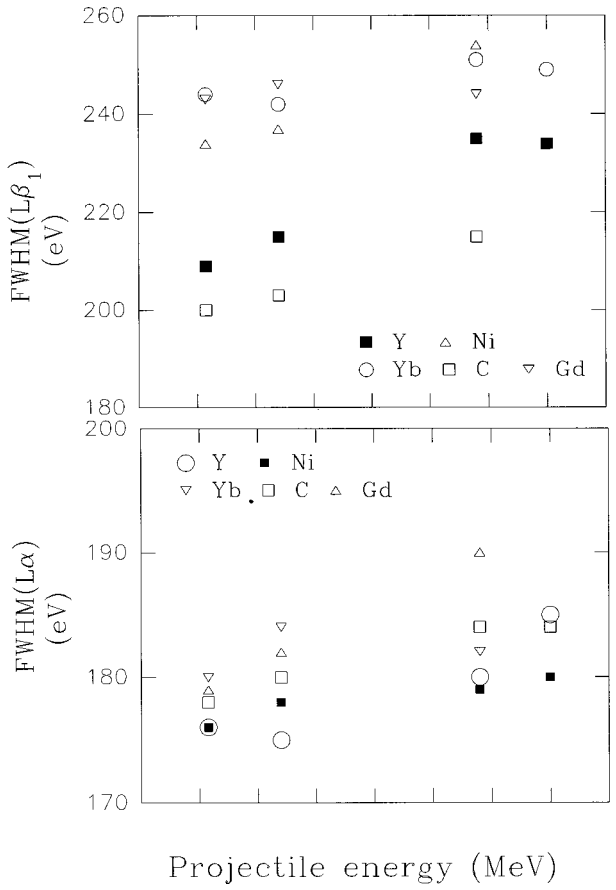

FIG. 7. The variation of the fitted FWHM of the $L\beta_1$ and $L\alpha$ lines of the I projectile with the incident energy, for a few targets. Typical errors are $<10\%$ in each case.

by Datz *et al.* are using thick targets and there is a slight difference in the projectile energies used. To bring out the salient features in the variations of $L\beta_1$-to-$L\alpha$ intensity ratio over a wide range of impact energies, it was therefore appropriate to normalize the data of Datz *et al.* to our observed results at an impact energy 60 MeV. These data taken as a whole show a variety of features depending upon the target atomic number.

For Ni, Yb, and Gd targets, which lie near the observed maxima in the $L\beta_1$-to-$L\alpha$ intensity ratio curve as a function of Z_2 (see Figs. 3–5), it is found that this ratio initially increases with energy, shows a maximum at around 60 MeV, and then decreases as the projectile energy increases (Fig. 6). On the other hand, for Ag and Pb, which are close to or at the minimum of this curve, this ratio continues to increase from 15- to 150-MeV projectile energy, initially at a faster rate. In the case of Y and Au targets, this ratio is almost energy independent whereas for C and Al, a decreasing trend at lower energies followed by a slow monotonic increase is observed.

TABLE I. The observed energies of the $L\alpha$ and $L\beta_1$ x rays from 63-MeV I projectile. The errors in the observed energy are within 10 eV.

Target	$L\alpha$ (eV)	$L\beta_1$ (eV)
C	4048	4413
Al	4073	4381
Ni	4062	4398
Se	4077	4413
Y	4071	4389
Ag	4075	4388
Gd	4073	4411
Yb	4081	4420
Au	4075	4389
Pb	4085	4398

Qualitative attempts to explain similar existing data on the periodic variation in the intensity ratio $L\beta_1$ to $L\alpha$ as a function of Z_2 have been made by Meyerhof *et al.* [25,26] and Hagmann *et al.* [18] and these have been reviewed by Wille and Hippler [27]. These explanations consider initial MO vacancy production at small internuclear distances through rotational couplings followed by vacancy sharing between the atomic levels of the collision partners through radial couplings at large internuclear distances on the outgoing branch of the collision. The relative vacancy production in $2p_{3/2}$ and $2s_{1/2}$ subshells of the projectile through vacancy sharing model follows a MO correlation rule, which depends on the atomic number Z_2 of the target. The radial coupling would be strong if the energy of the L shell matches with that of the K, L, or M level of the collision partner. For an I or Ag projectile, the vacancy sharing in the region $10<Z_2<40$ depends on K-L level matching condition. In the region $Z_2<20$, where the K-shell binding energy of the target is less than the L-shell binding enery of the projectile (''swapped case,'' see, e.g., MO correlation diagrams for Ar-Xe and Kr-Xe, Eichler *et al.* [28]), vacancy transfer from the $3d\sigma$ MO to the $2p_{3/2}$ subshell of the projectile is stronger than that to the $2s_{1/2}$ subshell of the projectile. For $20<Z_2<40$, the K-shell binding energy of the target is greater than the L-shell binding energy of the projectile (''unswapped case'' [28]). The vacancy is preferentially transferred from the $3d\sigma$ MO to the $2s_{1/2}$ subshell of the projectile. For $Z_2>40$, the L-L level matching condition is appropriate and initial vacancy in the $4f\sigma$ MO is preferentially transferred to the $2p_{3/2}$ subshell for near symmetric systems according to the correlation rule of Barat and Lichten [29] and with increasing asymmetry the correlation shifts from the $2p_{3/2}$ to the $2s_{1/2}$ subshell of the lighter collision partner (I or Ag projectile in this case) as shown by Eichler *et al.* [28]. The above qualitative arguments based on the coupling between selected MOs show the correct trend of the variation of the intensity ratio $L\beta_1$ to $L\alpha$ as a function of Z_2.

A stringent test of the theoretical arguments, however, would be their ability to explain the variation in the intensity ratio $L\beta_1$ to $L\alpha$ as a function of the impact energy for a given collision system since the radial coupling strongly depends on the relative velocity. In general, the theoretical models due to Meyerhof *et al.* [25,26] cannot explain well this energy dependence even qualitatively. We have made similar calculations for a few selected systems using the model of Meyerhof *et al.* [25,26] [see Eqs. (30), (31), and (34) in [25] and Eqs. (10) and (11) in [26]] using the ionization energy of that of the equilibrium charge state of the ion. The value of the Nikitin angle θ_k needed in this calculation

was varied around 90° to explore the predictions about the energy dependence. $\theta_k = 90°$ was used for the final calculation since it was found that the variation in the intensity ratio was not very sensitive to θ_k. In Fig. 6, we show our experimental results along with the work of Datz *et al.* [17] on the dependence of the intensity ratio $L\beta_1$ to $L\alpha$ of the I projectile on the impact energy over a large range, not reported so far and also our calculations based on the model of Meyerhof *et al.* [25,26]. It can be seen that for near symmetric collision (I→Ag), the prediction [curve marked (2) in Fig. 6(a)] of this model using the correlation rule of Barat *et al.* [29] for $4f\sigma$ MO explains the data qualitatively. However, these calculations [the dotted curve marked (2) in Fig. 6(a)] for asymmetric systems (I→Gd,Yb), using the correlation rule of Eichler *et al.* [28] for both $4f\sigma$ and $3d\sigma$ do not reproduce the data even qualitatively at low impact energy. It may be noted that for sufficiently asymmetric collision systems [I →Gd,Yb,Pb in Fig. 6(a)], contribution of a few percent to vacancy transfer to the L subshells from the $3d\sigma$ MO cannot be neglected as compared to that from the $4f\sigma$ [25]. The correlation rule of Eichler *et al.* [28] has been found to be valid for vacancy transfer from the dominant $4f\sigma$ MO [25] to the L subshells [25]. However, the correlation rule for the $3d\sigma$ is not conclusively established because of the lack of sufficient experimental evidence [25]. A possible explanation of the discrepancy at low impact energy could be that either the $3d\sigma$ follows the correlation rule of Barat *et al.* [29] or the model calculations of radial couplings for $4f\sigma$ and $3d\sigma$ using Demkov [30] formalism are not good enough. From Fig. 6(b), it is also observed that the calculation [26] for I →Ni under K-L level matching condition does not reproduce the experimental data even qualitatively. In short, the present theoretical understanding of the vacancy sharing in terms of the two-state models [25,26] is not sufficiently good.

A semiclassical impact-parameter–based coupled channel calculation with a basis containing reasonably large number of MOs needs to be performed to have a better understanding of the previous experimental data and the observations in the present work.

We have also observed the L x rays of Ag in collision with Ni and Se. For the same impact velocity, the role of the target and the projectile was interchanged to see if the outer-shell electronic configuration of the emitter has any significant effect on the observed $L\beta_1$-to-$L\alpha$ intensity ratio. The results are shown in Table II. In the case of Ni and Ag combination, the measured intensity ratio $L\beta_1$ to $L\alpha$ of the Ag x ray does not depend on whether the x-ray emitter is the target or the projectile, probably because Ni lies on the plateau (see Fig. 5) and hence is not very sensitive to the dynamical collision conditions. However, in the case of Se and Ag combination, Se being on the sharp slope of this curve (Fig. 5) any changes in the dynamical conditions might influence this variation strongly. The observed difference is difficult to explain on the basis of changes in the binding energies alone.

TABLE II. The measured value of the intensity ratio $L\beta_1$ to $L\alpha$ of Ag.

Energy/amu MeV	Projectile	Target	$L\beta_1$ to $L\alpha$
0.52	Ag	Ni	1.48(3)
0.57	Ni	Ag	1.46(3)
0.89	Ag	Ni	1.40(7)
0.93	Ni	Ag	1.50(2)
0.52	Ag	Se	0.82(2)
0.50	Se	Ag	1.10(3)
0.89	Ag	Se	0.98(2)
0.88	Se	Ag	1.16(3)

IV. CONCLUSION

The periodic variation in the $L\beta_1$-to-$L\alpha$ intensity ratio of I and Ag projectiles as a function of Z_2 is linked to the enhancement, through molecular orbitals, of the intensity of the $L\beta_3$ and $L\beta_4$ components, which are unresolved from the dominant $L\beta_1$ component. The theoretical calculations in terms of switching of correlation rule as a function of the atomic number of the collision partner in the two-state models do not explain the energy dependence of the vacancy transfer process satisfactorily. The intensity ratio $L\beta_1$ to $L\alpha$ is found to be slightly sensitive to the role of the emitter as the target or the projectile.

ACKNOWLEDGMENTS

The authors thank K. V. Thulasi Ram for his help during the experiments and the Pelletron staff for the smooth operation of the accelerator during the experiments. Thanks are also due to D. C. Ephraim and M.S. Dias for help during the preparation of the targets.

[1] R. K. Gardner and T. J. Gray, At. Data Nucl. Data Tables **21**, 515 (1978).
[2] D. D. Cohen, Nucl. Instrum. Methods Phys. Res. B **49**, 1 (1990).
[3] W. Brandt and G. Lapicki, Phys. Rev. A **20**, 465 (1979); **23**, 1717 (1981), and references therein.
[4] H. Paul and J. Muhr, Phys. Rep. **135**, 47 (1986).
[5] G. Lapicki, J. Phys. Chem. Ref. Data **18**, 111 (1989).
[6] J. A. Tanis, S. M. Shafroth, W. W. Jacobs, T. McAbee, and G. Lapicki, Phys. Rev. A **31**, 750 (1985).
[7] L. C. Tribedi, K. G. Prasad, P. N. Tandon, Z. Chen, and C. D. Lin, Phys. Rev. A **49**, 1015 (1994).
[8] L. Sarkadi and T. Mukoyama, J. Phys. B **13**, 2255 (1980).
[9] R. S. Sokhi and D. Crumpton, J. Phys. B **18**, 2871 (1985).
[10] L. Sarkadi and T. Mukoyama, Nucl. Instrum. Methods Phys. Res. B **61**, 167 (1990).
[11] H. C. Padhi, B. B. Dhal, V. Nanal, K. G. Prasad, P. N. Tandon, and D. Trautmann, Phys. Rev. A **54**, 3014 (1996), and references therein.
[12] L. Sarkadi and T. Mukoyama, J. Phys. B **14**, L255 (1981);

Nucl. Instrum. Methods Phys. Res. B **4**, 296 (1984).
[13] K. Finck, W. Jitschin, and H. O. Lutz, J. Phys. B **16**, L409 (1983).
[14] L. Sarkadi, J. Phys. B **19**, L755 (1986); **19**, 2519 (1986).
[15] L. Sarkadi and T. Mukoyama, J. Phys. B **20**, L559 (1987); Phys. Rev. A **37**, 4550 (1988).
[16] P. A. Amundsen and D. H. Jakubassa-Amundsen, J. Phys. B **21**, L99 (1988).
[17] S. Datz, C. D. Moak, B. R. Appleton, and T. A. Carlson, Phys. Rev. Lett. **27**, 363 (1971).
[18] S. Hagmann, P. Armbruster, G. Kraft, P. H. Mokler, and H.-J. Stein, J. Phys. A **288**, 353 (1978); **290**, 251 (1979).
[19] S. D. Narvekar, R. R. Hosangadi, L. C. Tribedi, R. G. Pillay, K. G. Prasad, and P. N. Tandon, Pramana **39**, 79 (1992).
[20] L. C. Tribedi, S. D. Narvekar, R. G. Pillay, and P. N. Tandon, Pramana **39**, 661 (1992).
[21] W. A. Schönfeldt, Ph. D. thesis GSI-81-7, 1981 (unpublished).
[22] B. Budick, J. Kast, and A. M. Rushton, Phys. Lett. **46A**, 137 (1973).
[23] D. D. Cohen and M. Harrigan, At. Data Nucl. Data Tables **34**, 393 (1986).
[24] Amal K. Saha (unpublished) .
[25] W. E. Meyerhof, A. Rüetschi, Ch. Stoller, M. Stöckli, and W. Wölfli, Phys. Rev. A **20**, 154 (1979).
[26] W. E. Meyerhof, R. Anholt, J. Eichler, and A. Salop, Phys. Rev. A **17**, 108 (1978).
[27] U. Wille and R. Hippler, Phys. Rep. **132**, 129 (1986).
[28] J. Eichler, U. Wille, B. Fastrup, and K. Taulbjerg, Phys. Rev. A **14**, 707 (1976).
[29] M. Barat and W. Lichten, Phys. Rev. A **6**, 211 (1972).
[30] Yu. N. Demkov, Zh. Eksp. Teor. Fiz. **45**, 195 (1963).